Inorg. Chem. **2004**, *43*, 1071–1081

Structural, Spectroscopic, and Electrochemical Studies of the Complexes $[Ni_2(\mu\text{-CNR})(CNR)_2(\mu\text{-dppm})_2]^{n+}$ (n = 0, 1, 2): Unusual Examples of Nickel(0)–Nickel(I) and Nickel(0)–Nickel(II) Mixed Valency

Gregory M. Ferrence,[†] Eugenio Simón-Manso,[‡] Brian K. Breedlove,[‡] Leah Meeuwenberg,[§] and Clifford P. Kubiak*[,‡]

Department of Chemistry & Biochemistry, University of California San Diego, La Jolla, California 92093-0358, and Department of Chemistry, Illinois State University, Normal, Illinois 61790

Received August 30, 2003

Reaction of $Ni(COD)_2$ (COD = cyclooctadiene) with dppm (dppm = bis(diphenylphosphino) methane) followed by addition of alkyl or aryl isocyanides yields the class of nickel(0) dimers $Ni_2(\mu\text{-CNR})(CNR)_2(\mu\text{-dppm})_2$ (R = CH_3 (**1**), n-C_4H_9 (**2**), $CH_2C_6H_5$ (**3**), i-C_3H_7 (**4**), C_6H_{11} (**5**), t-C_4H_9 (**6**), p-IC_6H_4 (**7**), 2,6-$(CH_3)_2C_6H_3$ (**8**)). The cyclic voltammograms of the dimers exhibit two sequential single electron oxidations to the +1 and +2 forms. Specular reflectance infrared spectroelectrochemical (IRSEC) measurements demonstrate reversible interconversions between the neutral Ni(0) dimers and their +1 and +2 forms. Bulk samples of the +2 forms are prepared by chemical oxidation using $[FeCp_2][PF_6]$, while the +1 forms are prepared by the comproportionation of neutral and +2 forms. The neutral complexes **6** and **8** were characterized by X-ray diffraction as symmetric, locally tetrahedral binuclear Ni(0) complexes. The +2 forms of these complexes, $\mathbf{6}^{2+}$ and $\mathbf{8}^{2+}$, have asymmetric structures with one locally square planar and one locally tetrahedral metal center, evidence for a Ni(II)–Ni(0) mixed valence state. The X-ray structural characterization of $\mathbf{6}^{+}$ is symmetrical and qualitatively similar to that of the neutral complex **6**. The +1 forms all exhibit intense near IR electronic absorptions that are assigned as intervalence charge transfer (IVCT) bands. On the basis of structural, spectroscopic, and electrochemical data, the +1 forms of the complexes, $\mathbf{1}^{+}$–$\mathbf{8}^{+}$, are assigned as Robin–Day class III, fully delocalized Ni(+0.5)–Ni(+0.5) mixed valence complexes.

Introduction

The d^{10}−d^{10}, dppm bridged dinuclear nickel complex $Ni_2(\mu\text{-CNCH}_3)(CNCH_3)_2(\mu\text{-dppm})_2$ (**1**) exhibits rich chemistry ranging from simple redox chemistry to transmetalation and multiple bond metathesis.[1−14] Previously, the oxidation of **1** to $\mathbf{1}^{2+}$ and several reactions of **1** with electrophiles were reported.[1−4] The bridging isocyanide of **1** can be alkylated with alkyl halides to form $[Ni_2(\mu\text{-CN(R)Me})(CNMe)_2(\mu\text{-dppm})_2]^{+}$.[1,2] CO_2 undergoes multiple bond metathesis with the carbon−nitrogen triple bonds of the isonitrile ligand to yield $Ni_2(\mu\text{-CO})(CO)_2(\mu\text{-dppm})_2$ and methyl isocyanate.[3,4] The bridging isonitrile of **1** is labile and is readily exchanged

* Author to whom correspondence should be addressed. E-mail: ckubiak@ucsd.edu.
[†] Illinois State University.
[‡] University of California San Diego.
[§] Visiting undergraduate from Kalamazoo College.

(1) DeLaet, D. L.; Fanwick, P. E.; Kubiak, C. P. *Organometallics* **1986**, *5*, 1807.
(2) Ratliff, K. S.; DeLaet, D. L.; Gao, J.; Fanwick, P. E.; Kubiak, C. P. *Inorg. Chem.* **1990**, *29*, 4022.
(3) DeLaet, D. L.; del Rosario, R.; Fanwick, P. E.; Kubiak, C. P. *J. Am. Chem. Soc.* **1987**, *109*, 754.
(4) DeLaet, D. L.; Fanwick, P. E.; Kubiak, C. P. *J. Chem. Soc., Chem. Commun.* **1987**, 1412.
(5) DeLaet, D. L.; Powell, D. R.; Kubiak, C. P. *Organometallics* **1985**, *4*, 954.
(6) Lemke, F. R.; DeLaet, D. L.; Gao, J.; Kubiak, C. P. *J. Am. Chem. Soc.* **1988**, *110*, 6904.
(7) Ratliff, K. S.; Broeker, G. K.; Fanwick, P. E.; Kubiak, C. P. *Angew. Chem., Int. Ed. Engl.* **1990**, *29*, 395.
(8) Gong, J.; Huang, J.; Fanwick, P. E.; Kubiak, C. P. *Angew. Chem., Int. Ed. Engl.* **1990**, *29*, 396.
(9) Ni, J.; Fanwick, P. E.; Kubiak, C. P. *Inorg. Chem.* **1988**, *27*, 2017.
(10) Ratliff, K. S.; Fanwick, P. E.; Kubiak, C. P. *Polyhedron* **1990**, *9*, 2651.
(11) Kim, H. P.; Fanwick, P. E.; Kubiak, C. P. *J. Organomet. Chem.* **1988**, *346*, C39.
(12) Kubiak, C. P.; Ratliff, K. S. *Isr. J. Chem.* **1991**, *31*, 3.
(13) Kubiak, C. P. In *Comprehensive Organometallic Chemistry II*; Abel, E. W., Stone, F. G. A., Wilkinson, G., Eds.; Pergamon: Tarrytown, 1995; Vol. 9.
(14) Morgenstern, D. A.; Ferrence, G. M.; Washington, J.; Rosenhein, L.; Henderson, J. I.; Heise, J. D.; Fanwick, P. E.; Kubiak, C. P. *J. Am. Chem. Soc.* **1996**, *118*, 2198.

10.1021/ic035021j CCC: $27.50
Published on Web 01/07/2004

Table 1. Data for $[Ni_2(\mu\text{-L})(L)_2(\mu\text{-dppm})_2]^{n+}$ ($n = 0, 1, 2$) Dimers

		^{31}P, ppm		ν(CN), cm^{-1}	
compound	L	$n = 0$	$n = 2+$	$n = 0$	$n = 2^+$
1	CH_3NC	18.3	35.2	2064, 1710	2196, 2085
2	n-C_4H_9NC	17.9	35.8	2051, 1698	2181, 2088
3	$C_6H_5CH_2NC$	18.6	36.2	2047, 1678	2184, 2097
5	$C_6H_{11}NC$	17.5	36.0	2047, 1712	2169, 2069
6	t-C_4H_9NC	17.3	10.2	2024, 1757	2169, 2078
7	p-IC_6H_4NC	20.7	36.2	1986, 1666	2135, 2020
8	xylylNC	20.4	9.49	2000,[a] 1820	2139, 2037

[a] Average.

with stronger π-acceptor ligands including aryl isocyanides and NO^+ to form $Ni_2(\mu\text{-CNAr})(CNMe)_2(\mu\text{-dppm})_2$ (Ar = aryl) and $[Ni_2(\mu\text{-NO})(CNMe)_2(\mu\text{-dppm})_2][PF_6]$, respectively.[2] **1** readily reacts with other metal containing species to form transmetalation products or larger clusters such as $[NiAu(CNMe)_2(\mu\text{-dppm})_2]Cl$ and $[\{Ni_2(\mu\text{-CNMe})(CNMe)_2(\mu\text{-dppm})\}_2Hg]^{2+}$, respectively.[8−11]

Prior to the studies presented here, no investigations of the effects of altering the isocyanide ligands have been reported. Similarly, the nature of the mixed valencies in the +1 and +2 states had not been characterized. Here, we report the synthesis of a series of nickel dimers, $[Ni_2(\mu\text{-CNR})(CNR)_2(\mu\text{-dppm})_2]$ (R = CH_3 (**1**), n-C_4H_9 (**2**), $CH_2C_6H_5$ (**3**), i-C_3H_7 (**4**), C_6H_{11} (**5**), t-C_4H_9 (**6**), p-IC_6H_4 (**7**), 2,6-$(CH_3)_2C_6H_3$ (**8**)) with aryl and alkyl isocyanides. X-ray crystallographic, electrochemical, and spectroscopic evidence for unusual $[Ni_2]^+$ and $[Ni_2]^{2+}$ mixed valence states are presented.

Results and Discussion

Synthesis and Structures of the Neutral Dimers $Ni_2(\mu\text{-CNR})(CNR)_2(\mu\text{-dppm})_2$. The nickel dimers $Ni_2(\mu\text{-CNR})(CNR)_2(\mu\text{-dppm})_2$ (R = CH_3 (**1**), n-C_4H_9 (**2**), $CH_2C_6H_5$ (**3**), i-C_3H_7 (**4**), C_6H_{11} (**5**), t-C_4H_9 (**6**), p-IC_6H_4 (**7**), 2,6-$(CH_3)_2C_6H_3$ (**8**)) were prepared in order to elucidate the electronic and steric effects of the isocyanide ligand on the structure and redox properties of this class of compounds. Each of the formally zerovalent nickel dimers **1**−**8** was synthesized by the room temperature addition of 3 equivalents of the appropriate isocyanide to a THF solution containing $Ni(COD)_2$ and dppm in a 1:1 ratio (eq 1).

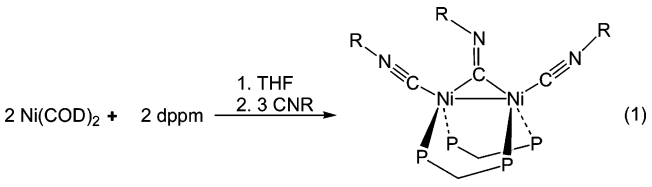

(1)

As the reaction proceeds, the solution changes from orange to red, and the products are obtained as orange to brick red solids (λ_{max} = 340−345 nm). Each of these complexes exhibits a single resonance at ca. 20 ± 2 ppm (Table 1) in the $^{31}P\{^1H\}$ NMR, which is similar to the related complex $Ni_2(\mu\text{-CO})(CO)_2(\mu\text{-dppm})_2$.[24,25] The small difference in chemical shift suggests that the nickel−phosphorus interaction is similar in each of the dimers.

In the solid state, each of the neutral dimers has one weak and one intense terminal ν(C≡N) stretching band above 2000 cm^{-1}, and a weak broad band below 2000 cm^{-1} corresponding to the bridging isocyanide ligand (Table 1). In solution, the terminal CN bands collapse to a single broad band. The terminal ν(C≡N) bands are not significantly affected by the nature of the alkyl or aryl group. Notable exceptions are complexes **6** and **8** with sterically demanding *tert*-butyl− and xylyl−isocyanide groups. The difference in the ν(C≡N) stretching frequencies for **6** and **8** suggests that the structures are somewhat different from the others due to the presence of the bulky isocyanides. This is borne out by the structural studies described below.

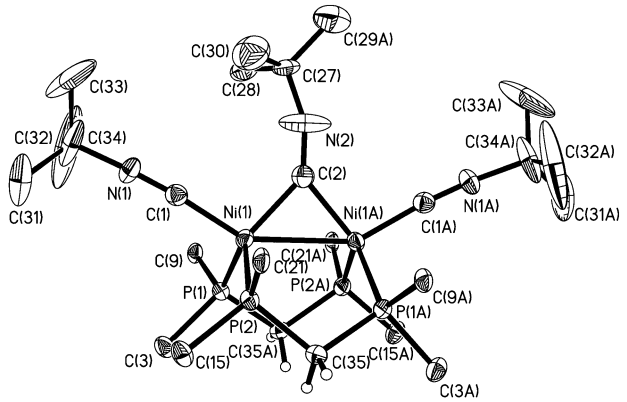

Figure 1. ORTEP plot of $Ni_2(\mu\text{-CN}(t\text{-}C_4H_9))(CN(t\text{-}C_4H_9))_2(\mu\text{-dppm})_2$ (**6**) showing 50% thermal ellipsoids.

The structures of **6** (*tert*-butyl) and **8** (2,6-xylyl) are shown in Figures 1 and 2, and selected bond lengths and angles are summarized in Table 4. Both complexes have overall "cradle" or "W-frame" type structures, and each Ni(0) center has an approximately tetrahedral coordination geometry with two phosphorus atoms from two bridging dppm ligands, one terminal isocyanide carbon atom, and one bridging isocyanide carbon atom forming the vertices. The average bond angles and bond distances about the nickel core in **6** and **8** are quite similar to those of **1**, but the steric bulk of the R group causes the C_{bridge}−N−C angle in **6** (159.0(2)°) and **8** (180°) to be quasi-linear and linear, respectively, compared to **1** (129.9(6)°). The C_{bridge}−N−C bond angle of 129.9(6)° and the reactivity of **1** are consistent with substantial sp^2 hybridization of the bridging isocyanide ligand,[1,2] whereas the linear nature of the bridging isocyanides of **6** and **8** are consistent with sp hybridization. The degree of sp^2 vs sp

(15) Wu, J.; Fanwick, P. E.; Kubiak, C. P. *Organometallics* **1987**, *6*, 1805−1807.
(16) Manojlovic-Muir, L.; Muir, K. W.; Davis, W. M.; Mirza, H. A.; Puddephatt, R. J. *Inorg. Chem.* **1992**, *31*, 904−909.
(17) Gong, J. K. Ph.D. Thesis, Purdue University, 1990.
(18) Gong, J. K.; Fanwick, P. E.; Kubiak, C. P. *J. Chem. Soc., Chem. Commun.* **1990**, 1190−1191.
(19) Hinze, S.; Gong, J.; Fanwick, P. E.; Kubiak, C. P. *J. Organomet. Chem.* **1993**, *458*, C10−C11.
(20) Fontaine, X. L. R.; Higgins, S. J.; Shaw, B. L.; Thornton-Pett, M.; Yichang, W. *J. Chem. Soc., Dalton Trans.* **1987**, 1501−1507.
(21) Morgenstern, D. A.; Bonham, C. C.; Rothwell, A. P.; Wood, K. V.; Kubiak, C. P. *Polyhedron* **1995**, *14*, 1129−1137.
(22) Ferrence, G. M.; Fanwick, P. E.; Kubiak, C. P. *Chem. Commun.* **1996**, 1575−1576.
(23) Maekawa, M.; Munakata, M.; Kuroda-Sowa, T.; Hachiya, K. *Inorg. Chim. Acta* **1995**, *233*, 1−4.
(24) Osborn, J. A.; Stanley, G. G.; Bird, P. H. *J. Am. Chem. Soc.* **1988**, *110*, 2117.
(25) Gong, J.; Kubiak, C. P. *Inorg. Chim. Acta* **1989**, *162*, 19.

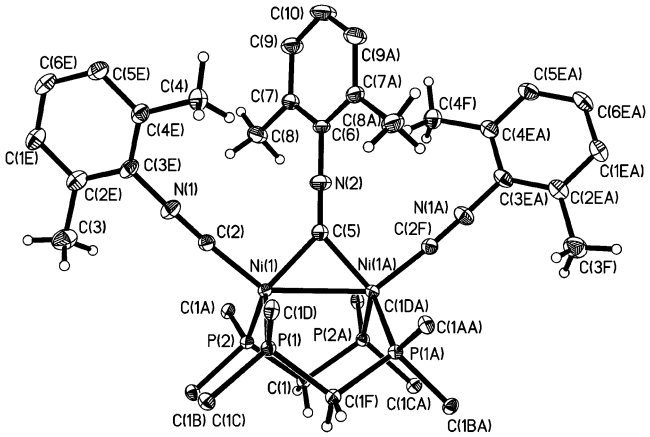

Figure 2. ORTEP plot of the complex $Ni_2(\mu\text{-CN}(2,6\text{-}(CH_3)_2C_6H_3))(CN(2,6\text{-}(CH_3)_2C_6H_3))_2(\mu\text{-dppm})_2$ (**8**) showing 50% thermal ellipsoids.

Table 2. Electrochemical Data for $[Ni_2(\mu\text{-L})(L)_2(\mu\text{-dppm})_2]^{n+}$ ($n = 0$, 1, 2) Species

compound	L	$E_{1/2}(2+/+)$ (V vs SCE)	$E_{1/2}(+/0)$ (V vs SCE)	ΔE (mV)	K_c
1	CH_3NC	−0.64	−1.00	360	1.2×10^6
2	*n*-C_4H_9NC	−0.60	−0.97	370	1.8×10^6
3	$C_6H_5CH_2NC$	−0.52	−0.85	330	3.7×10^5
4	*i*-C_3H_7NC	−0.62	−0.98	360	1.2×10^6
5	$C_6H_{11}NC$	−0.57	−0.99	420	1.2×10^7
6	*t*-C_4H_9NC	−0.50	−1.13	630	4.3×10^{10}
7	*p*-IC_6H_4NC	−0.25	−0.53	280	5.3×10^4
8	xylylNC	−0.19	−1.29	1100	3.7×10^{18}

character of the bridging ligand does appear to be correlated with the extent of Ni(0)-to-bridging ligand π-back-donation (vide infra).

The slightly longer $Ni-C_{bridge}$ (**6**, 1.925(3)Å; **8**, 1.927(2) vs **1**, 1.903(6)Å) and Ni−Ni (**8**, 2.6194(5) Å vs **1**, 2.572(1)Å) bond distances indicate net weaker metal−isocyanide interactions in **6** and **8** compared to **1**. The longer $Ni-C_{bridge}$ bond distances are also consistent with the observed higher bridging ν(C≡N) band energies of **6** (1757 cm^{-1}) and **8** (1820 cm^{-1}) compared to **1** (1710 cm^{-1}) and with a decrease in π-back-bonding. In the xylyl complex **8**, there is a pronounced twist of the xylyl ring (40°) with respect to the plane which contains the $Ni-C_{bridge}-Ni$ plane. This would be expected to reduce the overlap between Ni dπ and ligand π* orbitals of the bridging isocyanides and decrease π-back-bonding significantly.

Synthesis and Structures of the Divalent Dimers $[Ni_2(\mu\text{-CNR})(CNR)_2(\mu\text{-dppm})_2]^{2+}$. Addition of two equiv of ferrocenium hexafluorophosphate to an acetonitrile suspension of **1**−**8** resulted in the formation of solutions containing a mixture of ferrocene and the dicationic $[Ni_2]^{2+}$ product (eq 2). After ferrocene was extracted with benzene, the doubly

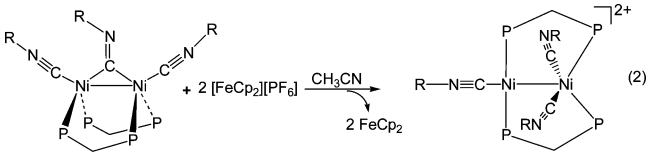

oxidized dimers $\mathbf{1}^{2+}$−$\mathbf{8}^{2+}$ were isolated as dark blue solids (λ_{max} = 580−590 nm) by recrystallization from methylene chloride/pentane. These +2 mixed valence complexes were

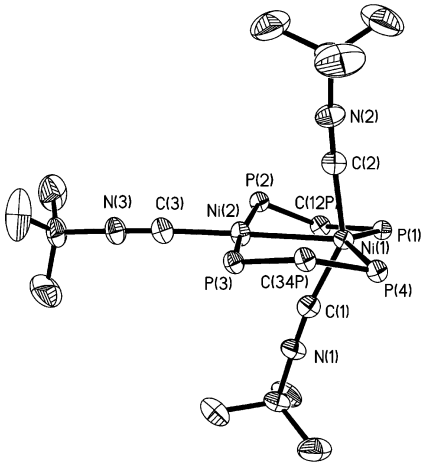

Figure 3. ORTEP plot of the complex $[Ni_2(\mu\text{-CN}(t\text{-}C_4H_9))(CN(t\text{-}C_4H_9))_2(\mu\text{-dppm})_2][PF_6]_2$ ($\mathbf{6}^{2+}$) showing 50% thermal ellipsoids.

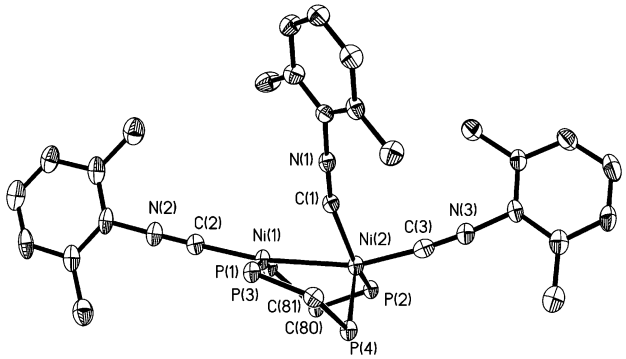

Figure 4. ORTEP plot of the complex $[Ni_2(\mu\text{-CN}(2,6\text{-}(CH_3)_2C_6H_3))(CN(2,6\text{-}(CH_3)_2C_6H_3))_2(\mu\text{-dppm})_2][PF_6]_2$ ($\mathbf{8}^{2+}$) showing 50% thermal ellipsoids.

then fully characterized. The two terminal isocyanide ligands give rise to IR absorption bands between 2130 and 2200 cm^{-1}, and the third isocyanide exhibits a semibridging mode ca. 100 cm^{-1} lower in energy.

The structures of $\mathbf{6}^{2+}$ and $\mathbf{8}^{2+}$ were determined by single-crystal X-ray diffraction. The structure of $[Ni_2(\mu\text{-CN}(t\text{-}C_4H_9))(CN(t\text{-}C_4H_9))_2(\mu\text{-dppm})_2][PF_6]_2$, $\mathbf{6}^{2+}$, and $[Ni_2(\mu\text{-CN}(2,6\text{-}(CH_3)_2C_6H_3)(CN(2,6\text{-}(CH_3)_2C_6H_3)_2(\mu\text{-dppm})_2][PF_6]_2$, $\mathbf{8}^{2+}$, are shown in Figures 3 and 4. Selected bond distances and angles are summarized in Table 4.

The structure of $\mathbf{6}^{2+}$ is essentially isostructural with $\mathbf{1}^{2+}$.[3] Generally, the Ni−L distances of $\mathbf{1}^{2+}$ and $\mathbf{6}^{2+}$ agree within experimental error. A notable exception is the longer Ni(2)−C(1) semibridging distance for $\mathbf{6}^{2+}$ (2.360(5) Å) compared to $\mathbf{1}^{2+}$ (2.19(1) Å), which may reflect the added bulk of the *tert*-butyl groups of $\mathbf{6}^{2+}$. Similarly the isocyanide C≡N distances do not differ significantly. All of the L−Ni−L angles in $\mathbf{6}^{2+}$ are within 12° of $\mathbf{1}^{2+}$. C−N−C bond angles are similar in both structures and are nearly linear. The structure of $\mathbf{6}^{2+}$ is best described as resulting from the dative interaction between a tetrahedral 18e$^-$, Ni^0L_4 fragment (Ni(1) in Figure 3) and a T-shaped, 14e$^-$, $Ni^{II}L_3$ fragment (Ni(2) in Figure 3).

The overall differences between the structures of $\mathbf{6}^{2+}$ and $\mathbf{8}^{2+}$ are in the pattern of substitution of the approximately tetrahedral nickel atom. In $\mathbf{6}^{2+}$, both of the isocyanides

Table 3. Crystal Data and Data Collection Parameters for **6**, $\mathbf{6}^{2+}$, $\mathbf{6}^{+}\cdot CH_2Cl_2$, **8**, and $\mathbf{8}^{2+}\cdot$THF

compound	**6**	$\mathbf{6}^{+}\cdot CH_2Cl_2$	$\mathbf{6}^{2+}$	**8**	$\mathbf{8}^{2+}\cdot$THF
formula	$C_{65}H_{71}N_3Ni_2P_4$	$C_{66}H_{73}Cl_2F_6N_3Ni_2P_5$	$C_{66}H_{74}Cl_2F_{12}N_3Ni_2P_6$	$C_{77}H_{71}N_3Ni_2P_4$	$C_{81}H_{79}F_{12}N_3Ni_2OP_6$
formula weight	1170.57	1365.52	1511.42	1281.68	1630.71
space group	*C*2/*c* (No. 15)	*P*1 (No. 1)	*C*2/*c* (No. 15)	*C*2/*c* (No. 15)	*P*2(1)/*n*
crystal system	monoclinic	triclinic	monoclinic	monoclinic	monoclinic
a, Å	23.657(5)	10.6578(7)	22.05(1)	21.4008(16)	13.8173(16)
b, Å	11.322(2)	13.3188(9)	16.34(1)	12.9100(10)	23.585(3)
c, Å	23.208(5)	13.5122(6)	40.28(3)	23.6900(18)	23.519(3)
α, deg	90	103.439(3)	90	90	90
β, deg	109.16(3)	101.316(3)	102.58(5)	106.6950(10)	100.956(2)
γ, deg	90	110.051(3)	90	90	90
V, Å^3	5872(2)	1670.6(4)	14164(15)	6269.3(8)	7524.7(15)
Z	4	1	8	4	4
d_{calc}, g cm^{-3}	1.324	1.357	1.418	1.358	1.439
crystal dimens, mm	0.25 × 0.22 × 0.12	0.44 × 0.40 × 0.38	2.00 × 0.60 × 0.35	0.80 × 0.20 × 0.12	0.4 × 0.2 × 0.10
temp, K	100(2)	193.	186.	100(2)	100(2)
F_{000}	2460	709.0	6232	2688	3372
GOF	1.074	1.030	1.049	0.950	0.978
final *R* indices [$I > 2\sigma(I)$] R_1	0.0324	0.042	0.0493	0.0364	0.0621

Table 4. Selected Bond Lengths (Å) and Angles (deg) for Compounds **6**, **8**, $\mathbf{6}^{2+}$, $\mathbf{8}^{2+}$, and $\mathbf{6}^{+}$

6		**8**		$\mathbf{6}^{2+}$		$\mathbf{8}^{2+}$		$\mathbf{6}^{+}$	
Ni(1)−Ni(1A)	2.5555(10)	Ni(1)−Ni(1A)	2.6194(5)	Ni(1)−Ni(2)	2.3931(13)	Ni(1)−Ni(2)	2.4813(10)	Ni(1)−Ni(2)	2.5879(8)
Ni(1)−C(1)	1.823(2)	Ni(1)−C(2)	1.8157(19)	Ni(1)−C(1)	1.847(5)	Ni(1)−C(2)	1.847(6)	Ni(1)−C(10)	1.859(6)
Ni(1)−C(2)	1.925(3)	Ni(1)−C(5)	1.927(2)	Ni(1)−C(2)	1.850(5)	Ni(1)−C(1)	2.436(5)	Ni(2)−C(30)	1.944(6)
C(2)−N(2)	1.202(5)	Ni(1)−P(2)	2.2046(5)	Ni(2)−P(2)	2.234(2)	Ni(1)−P(1)	2.2497(16)	Ni(1)−C(30)	2.009(6)
N(1)−C(1)	1.165(3)	N(1)−C(2)	1.155(3)	Ni(1)−P(4)	2.233(2)	Ni(1)−P(3)	2.2568(16)	Ni(2)−P(4)	2.2177(15)
Ni(1)−P(2)	2.1849(7)	N(2)−C(5)	1.206(4)	Ni(2)−C(1)	2.360(5)	Ni(2)−C(1)	1.843(6)	Ni(1)−P(3)	2.2141(15)
Ni(1)−P(1)	2.1911(7)	N(1)−C(3E)	1.3905(19)	Ni(1)−P(1)	2.234(2)	Ni(2)−C(3)	1.857(6)	N(10)−C(10)	1.170(8)
		N(2)−C(6)	1.359(4)	N(1)−C(1)	1.157(6)	Ni(2)−P(2)	2.2339(16)	N(20)−C(20)	1.155(7)
				N(2)−C(2)	1.146(6)	Ni(2)−P(4)	2.2356(16)	Ni(2)−C(20)	1.881(6)
				Ni(2)−C(3)	1.854(5)	N(2)−C(2)	1.160(7)	N(30)−C(30)	1.147(7)
				N(3)−C(3)	1.137(6)	N(2)−C(12)	1.415(7)		
						N(1)−C(1)	1.170(7)		
						N(1)−C(4)	1.421(7)		
C(1)−Ni(1)−C(2)	100.72(10)	C(2)−Ni(1)−C(5)	94.82(8)	C(1)−Ni(1)−C(2)	147.2(2)	P(1)−Ni(1)−P(3)	166.60(6)	C(10)−Ni(1)−C(30)	102.7(3)
P(2)−Ni(1)−P(1)	108.03(3)	C(2)−Ni(1)−P(1)	108.48(6)	C(1)−Ni(1)−P(4)	97.66(14)	C(2)−Ni(1)−P(3)	92.78(17)	P(3)−Ni(1)−P(1)	124.33(6)
C(1)−N(1)−C(34)	165.9(2)	C(2)−Ni(1)−P(2)	106.71(6)	C(2)−Ni(1)−P(4)	91.63(14)	C(2)−Ni(1)−P(1)	88.99(17)	P(4)−Ni(2)−P(2)	122.43(6)
C(2)−N(2)−C(27)	159.0(2)	P(1)−Ni(1)−P(2)	106.22(2)	C(1)−Ni(1)−P(1)	91.00(14)	P(2)−Ni(2)−P(4)	115.59(6)	C(20)−Ni(2)−C(30)	103.8(2)
N(1)−C(1)−Ni(1)	175.1(2)	C(2)−N(1)−C(3E)	175.3(2)	C(2)−Ni(1)−P(1)	104.5(2)	C(1)−Ni(2)−C(3)	93.5(2)	C(30)−Ni(2)−P(4)	112.98(17)
		C(5)−N(2)−C(6)	180	P(4)−Ni(1)−P(1)	134.79(6)	C(1)−N(1)−C(4)	170.9(5)	C(10)−N(10)−C(11)	171.3(7)
				P(4)−Ni(1)−Ni(2)	112.13(6)			C(20)−N(20)−C(21)	172.6(6)
				P(1)−Ni(1)−Ni(2)	111.95(5)			C(30)−N(30)−C(31)	175.4(7)
				C(3)−Ni(2)−Ni(1)	178.27(14)			N(30)−C(30)−Ni(1)	134.5(5)
				C(3)−Ni(2)−P(3)	94.39(14)				
				P(2)−Ni(2)−P(3)	170.39(5)				

coordinated to Ni(1) lean toward the other nickel atom in a semibridging manner. In $\mathbf{8}^{2+}$, only one of the isocyanides is semibridging. The other is oriented well away from Ni(2). This has the effect of producing a coordination geometry around Ni(1) in $\mathbf{8}^{2+}$ quite similar to that of the neutral "cradle" or "W-frame" type structure while the coordination geometry around Ni(2) becomes markedly more rectilinear

The oxidation of the dimers from $[Ni_2]^0$ to $[Ni_2]^{2+}$ leads to conversion of the *cis-cis* W-frame structure of $[Ni_2]^0$ into *trans-cis* structure of $[Ni_2]^{2+}$, breaking the symmetry between phosphorus atoms of the dppm ligand. The solution ^{31}P NMR spectra of all $[\mathbf{1}-\mathbf{8}]^{2+}$ complexes show a broad singlet at room temperature and an even sharper singlet below −90 °C (see Supporting Information). Since the ground-state structures for complexes $\mathbf{1}^{2+}$,[15] $\mathbf{6}^{2+}$, and $\mathbf{8}^{2+}$ (Figures 3 and 4) have two very different phosphorus environments, it is clear that in solution the complexes must be fluxional even at very low temperatures (Scheme 1). The simplest intramolecular mechanism which renders the phosphorus environment equivalent is the stepwise rotation of the three isocyanide ligands about the two nickel atoms, creating an effective symmetry plane perpendicular to the Ni−Ni axis. A close interaction between the C atom of the terminal ligand L1 (Scheme 1) and Ni(2) (Ni(2)−C(L1) = 2.789(5) Å) allows for direct interconversion of the bridging and terminal ligands.

Further information about the mechanism for exchange is obtained from the ^{1}H NMR spectra. At +35 °C, the CH_2P_2 unit of the dppm ligands and the *t*-C_4H_9 protons of the bridging and terminal isocyanide ligands give broad signals centered at [δ CH_aH_b, 2.95; δ Me, 2.2], and upon cooling the solution to −25 °C, the signal corresponding to the CH_2P_2 protons splits into an "AB" pattern [δH_a, 3.2; δH_b, 3.35 $^2J(H_aH_b) = 14$ Hz] and the signals corresponding to terminal and bridging isocyanides split into two broad singlets [δ CH_{3bridg}, 2.8; δ CH_{3term}, 2.6]. These data show that at low temperature (−25 °C) the fluxionality creates an effective plane of symmetry perpendicular to the Ni−Ni axis, thus

Scheme 1. Direct Interconversion of Terminal and Bridge Ligands by Rotation

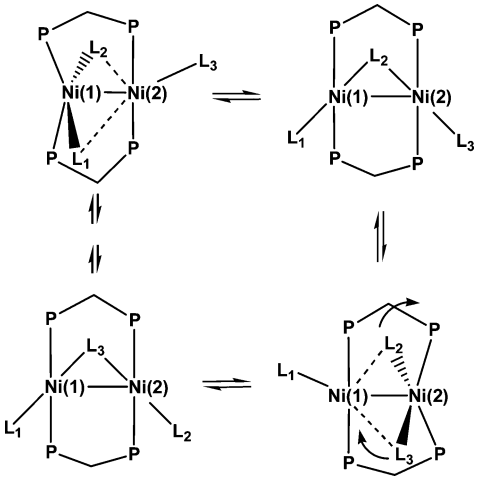

making the two nickel atoms and the four phosphorus atoms equivalent. It does not, however, create a plane of symmetry within the $Ni_2P_4C_2$ skeleton (Scheme 1). At higher temperature (+35 °C) the signals corresponding to CH_aH_b protons and the terminal and bridge isocyanide protons collapse, suggesting a fast exchange between terminal and bridging isocyanides and creating an effective plane of symmetry in the $Ni_2P_4C_2$ skeleton (Scheme 1). An analogous mechanism was proposed for the complexes $[Ni_2(\mu\text{-}CNMe)(CNMe)_2(\mu\text{-}dppm)_2][PF_6]_2$[5] and $Ni_2(\mu\text{-}CO)Cl_2(\mu\text{-}dppm)_2$.[16]

Infrared Spectroelectrochemistry of the Nickel Dimers. All of the dimers have two well-separated reversible single electron redox couples evident in their cyclic voltammograms (CV). The CV for **6** is presented in Figure 5. Table 2 summarizes the half-wave potentials and the observed splittings between the $E_{1/2}(+/0)$ and $E_{1/2}(2+/1+)$ for **1**−**8**. Compounds **1**−**5** show similar redox behavior, while **6**−**8** have larger separations between the two oxidation waves.

The conversion between the neutral and +2 oxidation states involves a $[Ni_2]^+$ species. To assess the structural trends in the $[Ni_2]^0$, $[Ni_2]^+$, and $[Ni_2]^{2+}$ states, we employed infrared spectroelectrochemistry (IRSEC). Figure 6 shows the isocyanide ν(CN) region of $Ni_2(\mu\text{-}CN(t\text{-}C_4H_9))(CN(t\text{-}C_4H_9))_2(\mu\text{-}dppm)_2$ (**6**) over the course of one SEC experiment. After the cell was charged with the neutral dimer, the potential was stepped to ca. −0.8 V vs SCE, halfway between the two redox potentials of **6**. The bands corresponding to the neutral dimer **6** at 2035 and 1745 cm^{-1} disappear as new bands appear at 2109 and 1976 cm^{-1} (Figure 6a). The potential is then stepped sufficiently positive ($E > -0.5$ V vs SEC) to generate the di-oxidized species $\mathbf{6}^{2+}$. The bands at 2109 and 1976 cm^{-1} decrease in intensity as the bands corresponding to $\mathbf{6}^{2+}$ appear (Figure 6b). Thus, the bands at 2109 and 1976 cm^{-1} correspond to $\mathbf{6}^+$. The +1 and neutral dimers are regenerated by stepping back to a sufficiently negative potential ($E < -1.1$ V vs SCE). Similar SEC experiments were carried out on the nickel dimers **1**, **2**, **3**, **5**, **6**, and **8**, and the IRSEC response for the oxidation of **1** is shown in Figure 7a. Here, bands at 1716 and 2072 cm^{-1} decrease as the band at 2141 cm^{-1} increases. Upon going to more positive potentials, Figure 7b, the band at 2141 cm^{-1} decreases as the band at 2194 cm^{-1} grows. Similar results were obtained for each of the dimers studied, and clean isosbestic points are observed for the terminal ν(C≡N) bands, indicating that conversion between oxidation states is direct and without the formation of any intermediates.

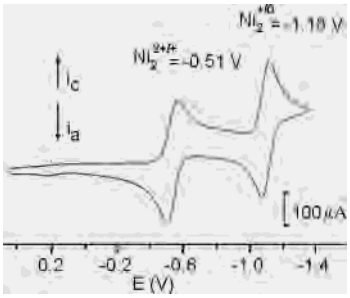

Figure 5. Cyclic voltammogram of the complex $[Ni_2(\mu\text{-}CN(t\text{-}C_4H_9))(CN(t\text{-}C_4H_9))_2(\mu\text{-}dppm)_2][PF_6]_2$ ($\mathbf{6}^{2+}$).

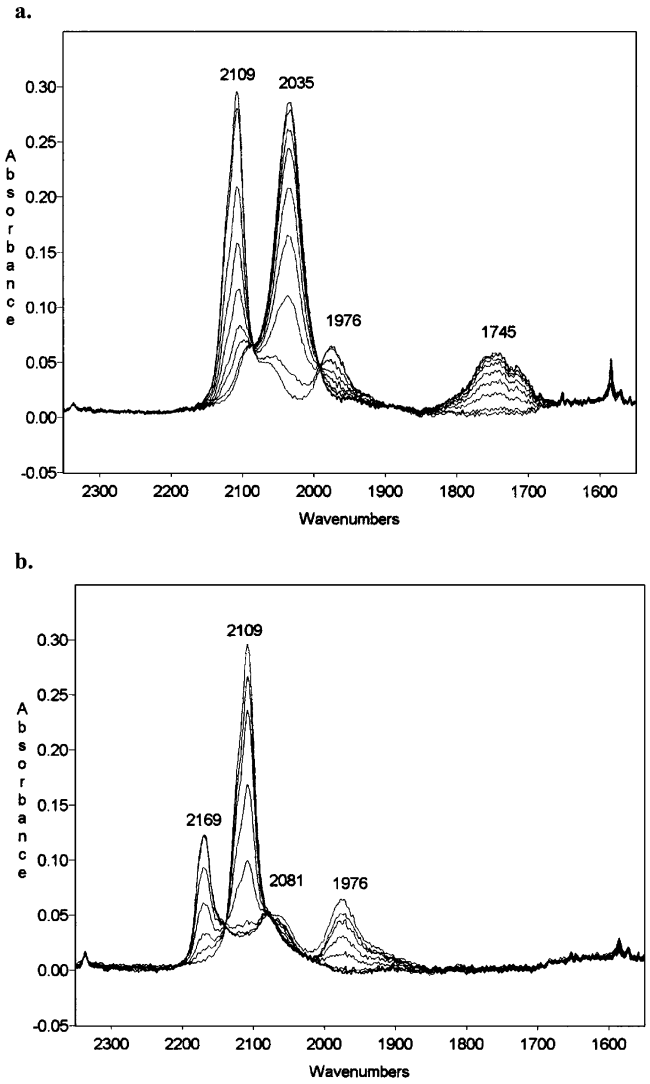

Figure 6. Infrared spectra from IRSEC of $[Ni_2(\mu\text{-}CN(t\text{-}C_4H_9))(CN(t\text{-}C_4H_9))_2(\mu\text{-}dppm)_2][PF_6]_2$, **6**: (a) oxidation of **6** to $\mathbf{6}^+$; (b) oxidation of $\mathbf{6}^+$ to $\mathbf{6}^{2+}$.

The one electron oxidized dimers $[Ni_2(\mu\text{-}CNR)(CNR)_2(\mu\text{-}dppm)_2]^+$ formally contain a $[Ni_2]^+$ core, suggesting the possibility of a Ni^0, Ni^I formal oxidation state. The character of this mixed valency is considered more carefully in the

next section. The terminal ν(C≡N) infrared stretching frequencies show a similar shift in energy of 65 ± 10 cm^{-1} upon removal of each subsequent electron. This is consistent with a decrease in π-back-bonding between the nickel and isocyanide carbon in progressively higher oxidation states. The bridging ν(C≡N) stretching frequencies are affected to a much larger degree, and generally changes in bridging ν(C≡N) stretching frequency are significantly greater upon oxidation from $[Ni_2]^0$ to $[Ni_2]^+$ as compared to oxidation from $[Ni_2]^+$ to $[Ni_2]^{2+}$. These results give further evidence for the HOMO of **1** being partially metal and substantially bridging C≡N based.[2]

Preparation of One Electron Oxidized $[Ni_2(\mu\text{-CNR})(CNR)_2(\mu\text{-dppm})_2]^+$ Dimers and X-ray Structural Characterization of $[Ni_2(\mu\text{-CN}(t\text{-}C_4H_9))(CN(t\text{-}C_4H_9))_2(\mu\text{-dppm})_2][PF_6]$. It is possible to prepare the one electron oxidized dimers $\mathbf{1}^+$−$\mathbf{8}^+$ by the comproportionation of the neutral and divalent states, eq 3. The ν(C≡N) stretching frequencies (KBr pellets) are similar to the corresponding values observed in the SEC experiments.

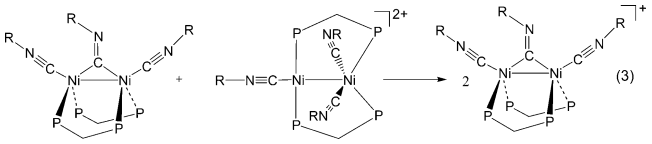

The structure of $\mathbf{6}^+$ is shown in Figure 8. The shift in bridging ν(C≡N) stretching frequencies upon oxidation from **6** to $\mathbf{6}^+$ is substantial (200 cm^{-1}). Indeed, a ν(C≡N) frequency of 1976 cm^{-1} is more typical of a semibridging isocyanide, like that in $\mathbf{6}^{2+}$, than the symmetrically bridging isocyanide found in **6**. However, the structure of $\mathbf{6}^+$ is remarkably similar to that of **6**, including the presence of a symmetrical bridging isocyanide ligand. The bond angles and distances of $\mathbf{6}^+$, Table 4, are also within experimental error of those of **6**!

The similarities in the structures of **6** and $\mathbf{6}^+$ suggest that the charge is evenly distributed over both metal centers, and possibly the ligands. Previous molecular orbital studies involving the model complex $[Ni_2(\mu\text{-CNH})(CNH)_2(\mu\text{-}PH_2CH_2PH_2)_2]$ showed that the HOMO involves the π^* orbital of the bridging isocyanide and Ni_2 dπ^* orbitals.[2] The HOMO involves a metal-to-ligand interaction of a type that can be considered the two metal−bridging ligand version of the usual Dewar−Chatt−Duncanson back-bonding model, see Figure 11, for example. Thus, removal of an electron should result in a significant reduction of π-back-bonding to the bridging isocyanide and a shortening of the CN triple bond. Only a slight shortening actually occurs on going from **6** (1.202(5) Å) to $\mathbf{6}^+$ (1.147(9) Å). The symmetric structure suggests a fully delocalized mixed valence description. Spectroscopic evidence for a Ni(+0.5)−Ni(+0.5) fully delocalized $[Ni_2]^+$ core is discussed later.

Stability of the One Electron Oxidized Nickel Dimer, $[Ni_2(\mu\text{-CNR})(CNR)_2(\mu\text{-dppm})_2]^+$. While the nature of the isocyanide ligand generally has little effect upon the structures of the neutral series of complexes, a profound effect on the electrochemistry of the dimers is observed. The values

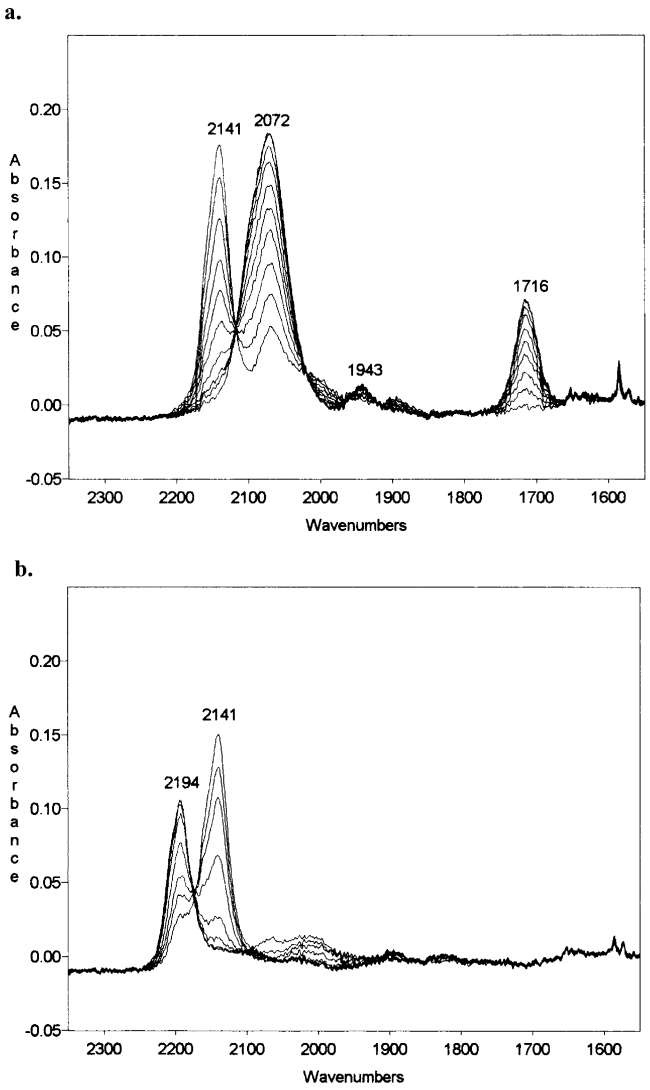

Figure 7. Infrared spectra from IRSEC of $[Ni_2(\mu\text{-CNCH}_3)(CNCH_3)_2(\mu\text{-dppm})_2][PF_6]_2$, **1**: (a) oxidation of **1** to $\mathbf{1}^+$; (b) oxidation of $\mathbf{1}^+$ to $\mathbf{1}^{2+}$.

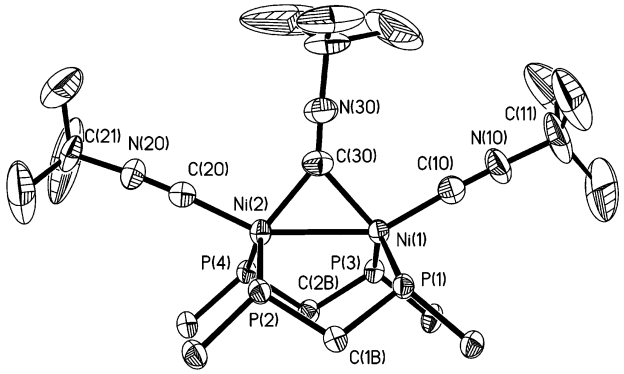

Figure 8. ORTEP plot of the complex $[Ni_2(\mu\text{-CN}(t\text{-}C_4H_9))(CN(t\text{-}C_4H_9))_2(\mu\text{-dppm})_2][PF_6]$ ($\mathbf{6}^+$) showing 50% thermal elllipsoids.

of $E_{1/2}$, ΔE, and the comproportionation equilibrium constant, K_C, for $[Ni_2(\mu\text{-CNR})(CNR)_2(\mu\text{-dppm})_2]$, **1**−**8**, are summarized in Table 2. The aliphatic substituted isocyanide dimers **1**−**5** exhibit similar $E_{1/2}(2+/+)$ and $E_{1/2}(+/0)$ values, and thus similar ΔE values that correspond to K_C on the order of 10^5 to 10^7. No particular correlations between electronic and steric factors for these ligands appear to exist. For **7**, R

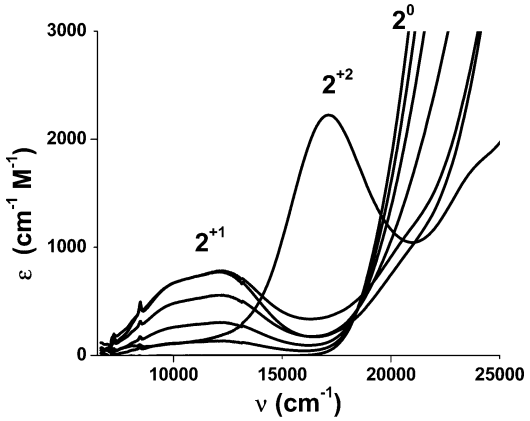

Figure 9. The comproportionation reaction of the two different oxidation states ($[Ni_2]^0 + [Ni_2]^{2+}$) for complex $Ni_2(\mu\text{-CN}(n\text{-}C_4H_9))(CN(n\text{-}C_4H_9))_2(\mu\text{-dppm})_2$ (**2**), monitored by UV−vis spectroscopy.

$= p\text{-}IC_6H_4$, single electron oxidation is significantly more positive than in dimers **1**−**6**, $E_{1/2}(0/+) = -0.25$ V vs SCE. Presumably, the aromatic ring helps to delocalize the electron density π-back-donated to the isocyanide more effectively, thus stabilizing the Ni(0) centers with respect to oxidation. Once formed, however, the one electron oxidized dimer readily loses the second electron to form the dication, $E_{1/2}(+/2+) = -0.25$ V vs SCE, thus the relatively small K_C, 5.3×10^4. Interestingly, the *tert*-butyl isocyanide dimer **6** and the xylyl isocyanide dimer **8** show markedly different electrochemistry and large increases in K_C, 10^{10} and 10^{18}, respectively. The first oxidations of these bulky dimers are 130−290 mV more cathodic than the other alkyl isocyanide based dimers. This indicates neutral states of decreased stability. Comparison of X-ray diffraction data of the **6** and **8** complexes to those of **1** indicates one substantial structural variation: the *quasi*-linear bridging isocyanide of **6** and completely linear isocyanide of **8**. The origin of the decreased stability of **6** and **8** toward oxidation appears to be simply that the bridging isocyanides which are forced sterically to be linear remain nominally sp hybridized. The bent (C−N−C, 129.9(6)°) bridging isocyanide of **1** can achieve nominal sp^2 hybridization through more effective back-donation. The "frustrated" back-donation to the bridging isocyanide ligands of **6** and **8** destabilizes these complexes with respect to oxidation. While the first oxidation of **6** is more cathodic than **1**, the second oxidation of **6** is comparable to the other aliphatic dimers. Hence $\mathbf{6}^+$ is stable over a large redox potential range, $K_C = 10^{10}$. The second oxidation of **8** is the most anodic of any of the compounds studied. This results in a very large K_C, 10^{18}. This is attributed to the ability of the aromatic rings of the xylyl isocyanides to stabilize the Ni(+0.5)−Ni(+0.5) mixed valence (+1) state.

UV−Vis Spectroscopy of the Nickel Dimers: Intervalence Charge Transfer. To further characterize the electronic structures of the unusual $[Ni_2]^+$ oxidation state of the nickel dimers, we investigated the UV−vis spectroscopy of $n\text{-}C_4H_9$ (sterically nonhindered, alkyl), $t\text{-}C_4H_9$ (sterically hindered, alkyl), and xylyl (sterically hindered, aromatic) as representatives of the group. The UV−visible spectral data for the complexes $[Ni_2(\mu\text{-CNR})(CNR)_2(\mu\text{-dppm})_2]^+$ are collected in Table 5. Figure 9 shows the comproportionation reaction (eq 3) for complex $Ni_2(\mu\text{-CN}(n\text{-}C_4H_9))(CN(n\text{-}C_4H_9))_2(\mu\text{-dppm})_2$ (**2**), monitored by UV−visible spectroscopy. In each of the examples, comproportionation reactions were accompanied by clean isosbestic points, indicating that

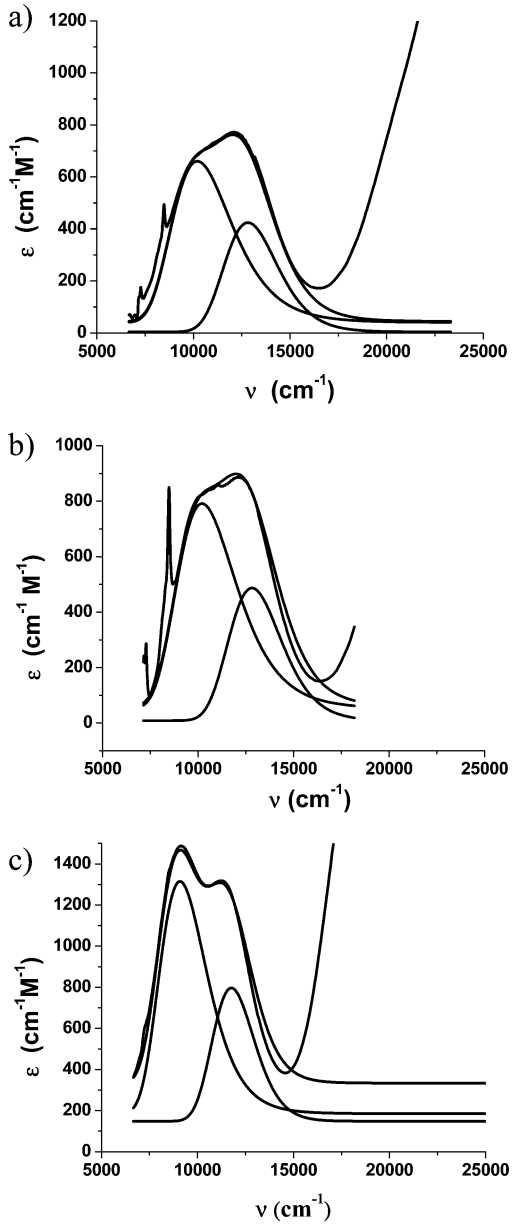

Figure 10. The experimental and simulated UV−vis spectra for the complexes $[Ni_2(\mu\text{-CNR})(CNR)_2(\mu\text{-dppm})_2][PF_6]$: (a) R = $n\text{-}C_4H_9$ ($\mathbf{2}^+$); (b) R = t-Bu ($\mathbf{6}^+$); (c) R = 2,6-$(CH_3)_2C_6H_3$ ($\mathbf{8}^+$).

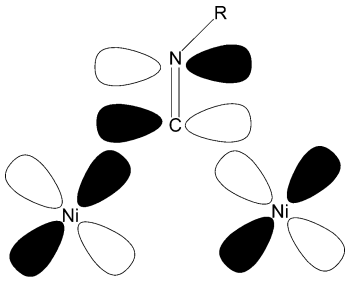

Figure 11. Orbital overlap diagram for the Ni_2 dπ*/ bridging ligand π* combination that describes the HOMO in **1**−**8**.

Table 5. Summary of Electronic Spectral Data for the Two IVCT Bands of the Mixed Valence [ ]$^+$ State of the Complexes $[Ni_2(\mu\text{-CNR})(CNR)_2(\mu\text{-dppm})_2][PF_6]$

R	ν_{max} (cm^{-1})	$\epsilon_{\nu max}$	$\Delta\nu_{1/2}$	H_{AB}[43]	ν_{max} (cm^{-1})	$\epsilon_{\nu max}$	$\Delta\nu_{1/2}$	H_{AB}[43]
n-C_4H_9 (**2**)	10101	658	3787	1260.6	12820	424	3295	1063.4
t-C_4H_9 (**6**)	10266	790	3926	1413.5	12787	486	3273	1129.8
xylyl (**8**)	9090	1314	3327	1598.8	11750	796	3057	1359.4

conversion between oxidation states is direct and without the formation of any intermediates, as was also observed in the IRSEC experiments. Figure 10 shows the broad electronic absorptions that appeared in the near IR region [6000−12000 cm^{-1}]. Assuming a Gaussian shape for a single IVCT band, the experimental spectra were simulated. The ν_{max}, extinction coefficient, $\nu_{1/2}$, and derived electronic coupling constant (H_{AB}) obtained from the spectra are summarized in Table 5. All three complexes exhibit multiple IVCT bands in this region. The *n*-C_4H_9 [10101 (658), 12820 (424) cm^{-1} (M^{-1} cm^{-1})] and *t*-C_4H_9 isocyanide complex [10266 (790), 12787 (486) cm^{-1} (M^{-1} cm^{-1})] bands appear at higher energy and at approximately half the intensity compared to the xylyl complex [9090 (1314), 11750 (796) cm^{-1} (M^{-1} cm^{-1})]. The energy difference between the two IT transitions shifts from 2521 cm^{-1} for *t*-C_4H_9 to 2719 cm^{-1} for *n*-C_4H_9. The IVCT band shape was examined in three different solvents (CH_3CN, THF, CH_2Cl_2) and showed no solvent dependence. There are several well studied complexes which exhibit multiple IVCT bands[4226−43] in Ru(II)−Os(III) and Ru(II)−Ru(III) systems. The multiplicity of the IVCT band was explained to arise from a ground state split by spin−orbit coupling. The origins of the split IVCT bands in the $[Ni_2]^+$ species may well be similar, as the SOMO is expected to be the Ni_2 dπ*/bridging ligand π* combination that could develop significant spin−orbit coupling, Figure 11.

Conclusions

A series of Ni dimers, $[Ni_2(\mu\text{-CNR})(CNR)_2(\mu\text{-dppm})_2]$, were synthesized by reacting $Ni(COD)_2$, dppm, and the appropriate isocyanide. As the steric bulk of the bridging isocyanide becomes progressively greater, the bridging ligand is prevented from adopting a bent geometry. This is reflected in $C_{bridge}-N-C$ angles of 159.0(2)° in the *tert*-butyl derivative (**6**) and 180° in the xylyl derivative (**8**), compared to 129.9(6)° in the methyl isocyanide complex (**1**). Electrochemical studies indicate that increased degrees of bending of the bridging isocyanide ligand stabilize the neutral Ni(0)−Ni(0) state with respect to oxidation. This is interpreted in terms of more effective Ni(0) to bridging ligand π* back-donation when the isocyanide ligand can bend to near 120°. Cyclic voltammetry combined with IRSEC experiments showed that three stable oxidation states exist for the dimers. Both the +2 and +1 states are accessible and can be isolated in pure form. The +2 state is assigned to a Ni(0)−Ni(II) mixed valency, based on X-ray crystal structures of $\mathbf{6}^{2+}$ and $\mathbf{8}^{2+}$ that show a locally tetrahedral coordination geometry about one nickel center and a locally T-shaped coordination geometry about the other. A dative nickel−nickel bond is presumed in these complexes. NMR studies reveal that the fluctuation between the localized Ni(0)−Ni(II) valencies is occurring on a time scale which is fast, even below −90° C. The +1 state is assigned to a formally Ni(+0.5)−Ni(+0.5) fully delocalized, Robin−Day class III classification. The structure of $\mathbf{6}^+$ is found to be completely symmetric, and is similar overall to the structure of **6**. The +1 states are found to be enormously stable. Comproportionation equilibrium constants express the relative stability of the +1 state with respect to the neutral and +2 states; and these are found to be as high as 10^{10} for **6** and 10^{18} for **8**. The +1 compounds all show multiple intervalence charge transfer bands in the near IR. These show no solvent dependence and most likely arise from a ground state split by spin−orbit coupling.

Experimental Section

General Information. All manipulations were performed under an N_2 atmosphere using an inert atmosphere glovebox or Schlenk techniques. Solvents were reagent or HPLC grade and dried over the appropriate drying agents. 2,6-Dimethylphenyl isocyanide was purchased from Fluka. Dppm, *n*-butyl isocyanide, *tert*-butyl isocyanide, cyclohexyl isocyanide, and benzyl isocyanide were purchased from Aldrich. All materials were used as received. $Ni(COD)_2$[25,26] and methyl isocyanide[27] were prepared by literature methods. *p*-IC_6H_4NC was prepared by the carbene method from the corresponding amine.[28] ^1H and ^{31}P NMR spectra were obtained using Varian XL-200 or General Electric QE-300 spectrometers. ^{31}P chemical shifts were referenced with respect to external 85% H_3PO_4. All NMR spectra were obtained in CD_2Cl_2 unless otherwise noted. Cyclic voltammetry was performed in acetonitrile or THF containing 0.1 M tetrabutylammonium hexafluorophosphate (TBAH) using a Princeton Applied Research model 173 potentiostat/galvanostat and model 175 universal programmer. A gold working electrode, a platinum wire counter electrode, and a ferrocene/ferrocenium reference electrode were employed. ^{31}P NMR and solid

(26) DeLaet, D. L. Ph.D. Thesis, Purdue University, 1987.
(27) Schunn, R. A.; Ittel, S. D.; Cushing, M. A. In *Inorganic Syntheses*; Angelici, R. J., Ed; Wiley: New York: 1990; Vol. 28, pp 94−98.
(28) Guerrieri, F.; Salerno, G. *J. Organomet. Chem.* **1976**, *114*, 339.
(29) Casanova, J.; Schuster, R. E.; Werner, N. D. *J. Chem. Soc.* **1963**, 4280.
(30) Weber, W. P.; Gokel, G. W. *Tetrahedron Lett.* **1972**, *17*, 1637.
(31) Wittrig, R. E.; Kubiak, C. P. *J. Electroanal. Chem.* **1995**, *393*, 75.
(32) McArdle, P. C. *J. Appl. Crystallogr.* **1996**, *239*, 306.
(33) Otwinowski, Z.; Minor, W. *Methods Enzymol.* **1996**, *276*, 307.
(34) Altomare, A.; Cascarano, G.; Giacovazzo, C.; Guagliardi, A.; Moliterni, A. G. G.; Burla, M. C.; Polidori, G.; Camalli, M.; Spagna, R. In preparation.
(35) *International Tables for Crystallography*; Kluwer Academic Publishers: Dordrecht, The Netherlands, 1992; Vol. C, Tables 4.2.6.8 and 6.1.1.4.
(36) Sheldrick, G. M. *SHELXS97. A Program for Crystal Structure Refinement*; University of Göttingen: Göttingen, Germany, 1997.
(37) Johnson, C. K. *ORTEPII*; Report ORNL-5138; Oak Ridge National Laboratory: Oak Ridge, TN, 1976.
(38) Spek, A. L. *PLUTON. Molecular Graphics Program*; University of Utrecht: Utrecht, The Netherlands, 1991.
(39) Hall, S. R., duBoulay, D., Eds. *Xtal_GX Package*; University of Western Australia: Australia, 1995.
(40) Beurskens, P. T.; Admirall, G.; Beurskens, G.; Bosman, W. P.; Garcia-Granda, S.; Gould, R. O.; Smits, J. M. M.; Smykalla, C. *The DIRDIF92 Program System*; Technical Report; Crystallography Laboratory, University of Nijmegen: Nijmegen, The Netherlands, 1992.
(41) Flack, H. D. *Acta Crystallogr.* **1983**, *A39*, 876.
(42) Haga, M.; Matsumura-Inoue, T.; Yamabe, S. *Inorg. Chem.* **1987**, *26*, 4148−4154 and references therein.
(43) Hush, N. S. *Prog. Inorg. Chem.* **1967**, *8*, 391.

state FT-IR data for the neutral and dication dimers are collected in Table 1. Electrochemical data for the dimers are collected in Table 2.

General Procedure for Preparation of $Ni_2(\mu\text{-}L)(L)_2(\mu\text{-}dppm)_2$. A method adapted from the preparation developed by Gong was followed.[17] To a stirred THF (ca. 50 mL THF per 1 g $Ni(COD)_2$) solution containing two equiv of $Ni(COD)_2$ and two equiv of dppm was added three equiv of the appropriate isocyanide (**L**), giving an orange-red solution. The solution was stirred for 1 h, during which time a red solid began to precipitate. Hexanes (ca. 150 mL) were added to precipitate an orange solid. The mixture was filtered through a frit, and the isolated solid was rinsed with hexanes and then CH_3CN to remove an orange-brown impurity. The solid red product $Ni_2(\mu\text{-}L)(L)_2(\mu\text{-}dppm)_2$ was then dried in vacuo. The product was recrystallized from THF/hexanes or toluene/hexanes as needed.

L = $CNCH_3$ (1). Following a method similar to the preparation of $Ni_2(\mu\text{-}L)(L)_2(\mu\text{-}dppm)_2$, $Ni(COD)_2$ (2.1 g, 7.6 mmol), dppm (2.9 g, 7.6 mmol), and methyl isocyanide (0.65 mL, 0.45 g, 10.9 mmol) gave **1**. Yield: 3.2 g (84%). ^1H NMR (C_6D_6): δ 7.2−8.2 (m, 40H, (C_6H_5)P), 4.0 (m, 4 H, PCH_2P), 2.8 (s, 6H, CH_3), 1.8 (m, 3H, CH_3).

L = $CN(n\text{-}C_4H_9)$ (2). Following a method similar to the preparation of $Ni_2(\mu\text{-}L)(L)_2(\mu\text{-}dppm)_2$, $Ni(COD)_2$ (1.0 g, 3.6 mmol), dppm (1.5 g, 3.9 mmol), and *n*-butyl isocyanide (0.57 mL, 0.45 g, 5.5 mmol) gave **2**. Yield: 1.2 g (60%). ^1H NMR (C_6D_6): δ 7.1−8.3 (m, 40H, (C_6H_5)P), 4.0 (m, 4 H, PCH_2P), 3.2 (m, 6H, CH_3), 2.3−2.7 (m, 3H, CH_3), 0.9−1.9 (m, 18H, CH_2). Anal. Calcd for $C_{65}H_{71}N_3Ni_2P_4$: C, 68.75; H, 6.30. Found: C, 68.82; H, 6.34.

L = $CNCH_2C_6H_5$ (3). Following a method similar to the preparation of $Ni_2(\mu\text{-}L)(L)_2(\mu\text{-}dppm)_2$, $Ni(COD)_2$ (1.0 g, 3.6 mmol), dppm (1.5 g, 3.9 mmol), and benzyl isocyanide (0.69 g, 5.9 mmol) gave **3**. Yield: 1.74 g (78%). ^1H NMR (C_6D_6): δ 7.1−8.3 (m, 55H, (C_6H_5)P, $C_6H_5CH_2$), 4.0 (m, 4 H, PCH_2P), 1.2−1.8 (m, 6H, CH_2). Anal. Calcd for $C_{74}H_{65}N_3Ni_2P_4$: C, 71.82; H, 5.29. Found: C, 71.47; H, 5.29.

L = $CN(i\text{-}C_3H_7)$ (4). Following a method similar to the preparation of $Ni_2(\mu\text{-}L)(L)_2(\mu\text{-}dppm)_2$, $Ni(COD)_2$ (1.0 g, 3.6 mmol), dppm (1.5 g, 3.9 mmol), and cyclohexyl isocyanide (0.50 mL, 0.38 g, 5.5 mmol) gave **4**. Yield: 1.77 g (89%).

L = CNC_6H_{11} (5). Following a method similar to the preparation of $Ni_2(\mu\text{-}L)(L)_2(\mu\text{-}dppm)_2$, $Ni(COD)_2$ (1.0 g, 3.6 mmol), dppm (1.5 g, 3.9 mmol), and cyclohexyl isocyanide (0.95 mL, 0.83 g, 7.6 mmol) gave **5**. Yield: 1.13 g (52%). ^1H NMR (C_6D_6): δ 7.1−8.3 (m, 40H, (C_6H_5)P), 4.0 (m, 4 H, PCH_2P), 1.2−3.7 (m of m, 33H, CH_2, CH_3).

L = $CN(t\text{-}C_4H_9)$ (6). Following a method similar to the preparation of $Ni_2(\mu\text{-}L)(L)_2(\mu\text{-}dppm)_2$, $Ni(COD)_2$ (1.0 g, 3.6 mmol), dppm (1.5 g, 3.9 mmol), and *tert*-butyl isocyanide (0.62 mL, 0.46 g, 5.5 mmol) gave **6**. Yield: 1.6 g (78%). ^1H NMR (C_6D_6): δ 7.0−8.5 (m, 40H, (C_6H_5)P), 4.0 (m, 4 H, PCH_2P), 1.0−2.5 (m, 27H, CH_2, CH_3). Anal. Calcd for $C_{65}H_{71}N_3Ni_2P_4$: C, 68.75; H, 6.30. Found: C, 68.72; H, 6.32.

L = $CN(p\text{-}IC_6H_4)$ (7). Following a method similar to the preparation of $Ni_2(\mu\text{-}L)(L)_2(\mu\text{-}dppm)_2$, $Ni(COD)_2$ (1.0 g, 3.6 mmol), dppm (1.5 g, 3.9 mmol), and *p*-iodophenyl isocyanide (1.4 g, 6.1 mmol) gave **7**. Yield: 1.9 g (69%).

L = $CN(2,6\text{-}(CH_3)_2C_6H_3)$ (8). Following a method similar to the preparation of $Ni_2(\mu\text{-}L)(L)_2(\mu\text{-}dppm)_2$, $Ni(COD)_2$ (1.00 g, 3.6 mmol), dppm (1.5 g, 3.9 mmol), and xylyl isocyanide (0.72 g, 5.5 mmol) gave **8**. Yield: 1.8 g (78%). $^{31}P\{^1H\}$ (THF): δ 20.4 (br, s). Anal. Calcd for $C_{77}H_{71}N_3Ni_2P_4$: C, 72.27; H, 5.59. Found: C, 72.09; H, 5.65.

General Procedure for Preparation of $[Ni_2(\mu\text{-}L)(L)_2(\mu\text{-}dppm)_2][PF_6]_2$. Two equivalents of $[FeCp_2][PF_6]$ was added to a stirred CH_3CN (ca.30 mL) solution of $Ni_2(\mu\text{-}L)(L)_2(\mu\text{-}dppm)_2$ (ca. 0.5 g). The dimer was initially suspended in the CH_3CN. As the reaction proceeded over 30 min, it reacted with the $[FeCp_2][PF_6]$, and the solution turned green as the soluble dicationic product was formed. The resulting solution mixture evaporated to dryness, and the $FeCp_2$ was removed by extraction with benzene. The product was dissolved in CH_2Cl_2, precipitated with pentane, and filtered to obtain pure $[Ni_2(\mu\text{-}L)(L)_2(\mu\text{-}dppm)_2][PF_6]_2$.

L = $CNCH_3$ ($\mathbf{1}^{2+}$). Following a method similar to the preparation of $[Ni_2(\mu\text{-}L)(L)_2(\mu\text{-}dppm)_2][PF_6]_2$ and previously reported, **1** (0.51 g, 0.51 mmol) and $[FeCp_2][PF_6]$ (0.33 g, 1.0 mmol) gave $\mathbf{1}^{2+}$. Anal. Calcd for $C_{64}H_{69}N_3Ni_2P_6F_{12}$: C, 53.25; H, 4.82. Found: C, 53.27; H, 4.84.[3] ^1H NMR (CD_3CN): δ 7.2−7.8 (m, 40H, (C_6H_5)P), 3.4−3.7 (m, 4 H, PCH_2P), 2.7 (m, 9H, CH_3).

L = $CN(n\text{-}C_4H_9)$ ($\mathbf{2}^{2+}$). Following a method similar to the preparation of $[Ni_2(\mu\text{-}L)(L)_2(\mu\text{-}dppm)_2][PF_6]_2$, **2** (0.51 g, 0.45 mmol) and $[FeCp_2][PF_6]$ (0.29 g, 0.88 mmol) gave $\mathbf{2}^{2+}$. ^1H NMR (CD_3CN): δ 7.2−7.8 (m, 40H, (C_6H_5)P), 3.5−3.7 (m, 4 H, PCH_2P), 0.4−1.1, 1.9, 2.1, 3.0 (m, m, s, s, 27H, CH_2, CH_2).

L = $CNCH_2C_6H_5$ ($\mathbf{3}^{2+}$). Following a method similar to the preparation of $[Ni_2(\mu\text{-}L)(L)_2(\mu\text{-}dppm)_2][PF_6]_2$, **3** (0.50 g, 0.40 mmol) and $[FeCp_2][PF_6]$ (0.27 g, 0.82 mmol) gave $\mathbf{3}^{2+}$. ^1H NMR (CD_3CN): δ 6.5−7.8 (m, 55H, (C_6H_5)P, $CH_2C_6H_5$), 3.3−3.7 (m, 4 H, PCH_2P), 4.2 (s, 6H,CH_2).

L = $CN(i\text{-}C_3H_7)$ ($\mathbf{4}^{2+}$). Following a method similar to the preparation of $[Ni_2(\mu\text{-}L)(L)_2(\mu\text{-}dppm)_2][PF_6]_2$, **4** (0.51 g, 0.47 mmol) and $[FeCp_2][PF_6]$ (0.30 g, 0.91 mmol) gave $\mathbf{4}^{2+}$.

L = CNC_6H_{11} ($\mathbf{5}^{2+}$). Following a method similar to the preparation of $[Ni_2(\mu\text{-}L)(L)_2(\mu\text{-}dppm)_2][PF_6]_2$, **5** (0.51 g, 0.42 mmol) and $[FeCp_2][PF_6]$ (0.27 g, 0.82 mmol) gave $\mathbf{5}^{2+}$. Anal. Calcd for $C_{71}H_{77}N_3Ni_2P_6F_{12}$: C, 56.72; H, 5.16. Found: C, 56.79; H, 5.29. ^1H NMR (CD_3CN): δ 7.2−7.8 (m, 40H, (C_6H_5)P), 3.0−3.7 (2m, 4 H, PCH_2P), 0.5−2.4 (m, 33H, CH, CH_2).

L = $CN(t\text{-}C_4H_9)$ ($\mathbf{6}^{2+}$). Following a method similar to the preparation of $[Ni_2(\mu\text{-}L)(L)_2(\mu\text{-}dppm)_2][PF_6]_2$, **6** (0.50 g, 0.44 mmol) and $[FeCp_2][PF_6]$ (0.29 g, 0.88 mmol) gave $\mathbf{6}^{2+}$. ^1H NMR (CD_3CN): δ 6.9−8.0 (m, 40H, (C_6H_5)P), 3.4−3.8 (m, 4 H, PCH_2P), 0.8 (br s, 27H, CH_3).

L = $CN(p\text{-}IC_6H_4)$ ($\mathbf{7}^{2+}$). Following a method similar to the preparation of $[Ni_2(\mu\text{-}L)(L)_2(\mu\text{-}dppm)_2][PF_6]_2$, **7** (0.50 g, 0.32 mmol) and $[FeCp_2][PF_6]$ (0.18 g, 0.54 mmol) gave $\mathbf{7}^{2+}$.

L = $CN(2,6\text{-}(CH_3)_2C_6H_3)$ ($\mathbf{8}^{2+}$). Following a method similar to the preparation of $[Ni_2(\mu\text{-}L)(L)_2(\mu\text{-}dppm)_2][PF_6]_2$, **8** (0.50 g, 0.30 mmol) and $[FeCp_2][PF_6]$ (0.18 g, 0.54 mmol) gave $\mathbf{8}^{2+}$. $^{31}P\{^1H\}$ (THF): δ 9.49(br, s).

Infrared Spectroelectrochemistry. The design of the reflectance IR spectroelectrochemical cell used in the nickel dimer study was reported previously by our laboratory.[31] Infrared spectral changes accompanying thin-layer bulk electrolyses were measured using a flow-through spectroelectrochemical cell. All spectroelectrochemical experiments were carried out using 5 mM THF solutions of $Ni_2(\mu\text{-}L)(L)_2(\mu\text{-}dppm)_2$ with 0.1 M TBAH as the supporting electrolyte. All solutions were prepared in a drybox and were degassed completely before injection into the spectroelectrochemical cell. Blank THF solutions of 0.1 M TBAH were used for the FT-IR difference spectra. A PAR model 175 universal programmer with a PAR model 176 current follower were used to effect and monitor thin layer bulk electrolyses. The IR spectra were acquired using a Mattson Research series FTIR with an external sampling port and a MCT (mercury−cadmium−telluride) detector.

Preparation of $[Ni_2(\mu\text{-CNR})(CNR)_2(\mu\text{-dppm})_2][PF_6]$ by Comproportionation. The preparation of $\mathbf{1}^+$ is representative for the preparation of each of the monocation nickel dimers. **1** (0.1 g, 0.10 mmol) was dissolved in ca. 20 mL of a 1:1 mixture of THF and CH_3CN. To this stirred solution was added $\mathbf{1}^{2+}$ (0.13 g, 0.10 mmol). The solution turned yellow/brown. After stirring for 0.5 h, $\mathbf{1}^+$ was isolated by evaporation of the reaction solution to dryness. KBr IR: $\mathbf{1}^+$ ($CNCH_3$), 2150, 1983 cm^{-1}; $\mathbf{2}^+$ ($CN(n\text{-}C_4H_9)$), 2117, 1995 cm^{-1}; $\mathbf{3}^+$ ($CNCH_2C_6H_5$), 2117, 1980 cm^{-1}; $\mathbf{5}^+$ (CNC_6H_{11}), 2109, 1987 cm^{-1}, $\mathbf{6}^+$ ($CN(t\text{-}C_4H_9)$), 2105, 1970 cm^{-1}; $\mathbf{7}^+$ ($p\text{-}IC_6H_4NC$), 2074, 1899 cm^{-1}. Elemental analysis was not obtained for the monooxidized dimers as it is difficult to obtain this oxidation state in bulk in the absence of either the dioxidized or neutral dimers.

General Procedures for UV−Vis Spectroscopy. All UV−visible experiments were performed using a UV−vis−NIR scanning spectrophotometer (UV-3101PC) and quartz cells with 1 cm path length sealed with a septum. To avoid dilution during comproportionation reactions, equimolar solutions were used. The following procedure is standard for all complexes. The $[Ni_2(\mu\text{-L})(L)_2(\mu\text{-dppm})_2]^+[PF_6]$ complex was obtained by comproportionation reaction of the neutral and +2 species. To 3 mL (0.1 mM) of the neutral complex $[Ni_2(\mu\text{-L})(L)_2(\mu\text{-dppm})_2]^0$ (L = *n*-BuNC, *t*-BuNC, 2,6-$(CH_3)_2C_6H_3NC$) was injected 3 mL (in 0.5 mL portions) of the $[Ni_2(\mu\text{-L})(L)_2(\mu\text{-dppm})_2]^{2+}[PF_6]_2$ (0.1 mM), and the UV−vis spectra were recorded.

X-ray Crystallography of $Ni_2(\mu\text{-}CN(t\text{-}C_4H_9))(CN(t\text{-}C_4H_9))_2(\mu\text{-dppm})_2$, 6. An orange plate of $C_{65}H_{71}Ni_2N_3P_4$ having approximate dimensions of 0.25 × 0.22 × 0.12 mm was mounted on a glass fiber in a random orientation. See Table 3 for a summary of crystal data and X-ray collection information. Selected bond lengths and angles are summarized in Table 4. Preliminary examination and data collection were performed with Mo Kα radiation ($\lambda = 0.71073$ Å) on a Nonius Kappa CCD. Cell constants and an orientation matrix for data collection were obtained from least-squares refinement, using the setting angles of 24791 reflections in the range $2° < \theta < 30°$. The monoclinic cell parameters and calculated volume are $a = 23.657(5)$ Å, $b = 11.322(2)$ Å, $c = 23.208(5)$ Å, $\beta = 109.16(3)°$, and $V = 5872(2)$ Å^3. For $Z = 4$ and fw = 1170.57 the calculated density is 1.324 g/cm^3. The space group was determined by the program ABSEN.[32] From the systematic presences of: $h0l$ $l = 2n$ and from subsequent least-squares refinement, the space group was determined to be monoclinic *C*2/*c* (No. 15).

The data were collected at a temperature of 100 ± 0.1 K and to a maximum 2θ of 55.0°. A total of 17682 reflections were collected, of which 4219 were unique [$R_{int} = 0.0571$]. Lorentz and polarization corrections were applied to the data. The linear absorption coefficient is 7.95 mm^{-1}/cm for Mo Kα radiation. An empirical absorption correction using SCALEPACK was applied.[33] Transmission coefficients ranged from 0.455 to 0.912 with an average value of 0.750. Intensities of equivalent reflections were averaged. The agreement factor for the averaging was 12.9% based on intensity. The structure was solved by direct methods using SIR97.[34] The remaining atoms were located in succeeding difference Fourier syntheses. Hydrogen atoms were included in the refinement but restrained to ride on the atom to which they are bonded. The structure was refined in full-matrix least-squares where the function minimized was $\sum w(|F_o|^2 - |F_c|^2)^2$ and the weight *w* is defined as $w = 1/[\sigma^2(F_o^2) + (0.0844P)^2 + 0.0000P]$ where $P = (F_o^2 + 2F_c^2)/3$.

Scattering factors were taken from the *International Tables for Crystallography*.[35] 7897 reflections were used in the refinements. However, only reflections with $F_o^2 > 2\sigma(F_o^2)$ were used in calculating *R*. The final cycle of refinement included 355 variable parameters and converged (largest parameter shift was 0.03 × esd) with unweighted and weighted agreement factors of $R_1 = \sum|F_o - F_c|/\sum F_o = 0.0324$ and $R_2 = (\sum w(F_o^2 - F_c^2)^2/\sum w(F_o^2)^2)^{1/2} = 0.0870$.

The standard deviation of an observation of unit weight was 0.96. The highest peak in the final difference Fourier had a height of 0.481 e/Å^3. The minimum negative peak had a height of −0.291 e/A^3. Refinement was performed on an AlphaServer 2100 using SHELX-97.[36] Crystallographic drawings were done using programs ORTEP,[37] PLUTON,[38] and/or Xtal_GX.[39]

X-ray Crystallography of $[Ni_2(\mu\text{-}CN(t\text{-}C_4H_9))(CN(t\text{-}C_4H_9))_2(\mu\text{-dppm})_2][PF_6]_2$, $\mathbf{6}^{2+}$. The key parameters are summarized in Table 3, and bond lengths and angles are summarized in Table 4. The refinement method was a full-matrix least-squares on F^2. The scan speed was 10 to 20°/minute with a 0.6°, Wyckoff range. The background range was 0.6° for 25% of the time, each side.

X-ray Crystallography of $[Ni_2(\mu\text{-}CN(t\text{-}C_4H_9))(CN(t\text{-}C_4H_9))_2(\mu\text{-dppm})_2][PF_6]\cdot CH_2Cl_2$, $\mathbf{6}^+\cdot CH_2Cl_2$. A dark red chunk of $C_{66}H_{73}Cl_2F_6N_3Ni_2P_5$ having approximate dimensions of 0.44 × 0.40 × 0.38 mm was mounted on a glass fiber in a random orientation. See Table 3 for a summary of crystal data and X-ray collection information. Selected bond lengths and angles are summarized in Table 4. Preliminary examination and data collection were performed with Mo Kα radiation ($\lambda = 0.71073$ Å) on a Nonius KappaCCD. Cell constants and an orientation matrix for data collection were obtained from least-squares refinement, using the setting angles of 13500 reflections in the range $4° < \theta < 27°$. The triclinic cell parameters and calculated volume are $a = 10.6578(7)$ Å, $b = 13.3188(9)$ Å, $c = 13.5122(6)$ Å, $\alpha = 103.439(3)°$, $\beta = 101.316(3)°$, $\gamma = 110.051(3)°$, and $V = 1670.6(4)$ Å^3. For $Z = 1$ and fw = 1365.52 the calculated density is 1.36 g/cm^3. The space group was determined by the program ABSEN.[32] There were no systematic absences, and the space group was determined to be *P*1 (No. 1).

The data were collected at a temperature of 193 ± 1 K and to a maximum 2θ of 55.0°. A total of 13500 reflections were collected, of which 8374 were unique. Lorentz and polarization corrections were applied to the data. The linear absorption coefficient is 8.2 /cm for Mo Kα radiation. An empirical absorption correction using SCALEPACK was applied.[33] Transmission coefficients ranged from 0.371 to 0.735 with an average value of 0.628. Intensities of equivalent reflections were averaged. The agreement factor for the averaging was 4.2% based on intensity. The structure was solved using the structure solution program PATTY in DIRDIF92.[40] The remaining atoms were located in succeeding difference Fourier syntheses. Hydrogen atoms were included in the refinement but restrained to ride on the atom to which they are bonded. The structure was refined in full-matrix least-squares where the function minimized was $\sum w(|F_o|^2 - |F_c|^2)^2$ and the weight *w* is defined as $w = 1/[\sigma^2(F_o^2) + (0.0481P)^2 + 1.9721P]$ where $P = (F_o^2 + 2F_c^2)/3$.

Scattering factors were taken from the *International Tables for Crystallography*.[35] 8374 reflections were used in the refinements. However, only reflections with $F_o^2 > 2\sigma(F_o^2)$ were used in calculating *R*. The final cycle of refinement included 766 variable parameters and converged (largest parameter shift was 0.05 times its esd) with unweighted and weighted agreement factors of $R_1 = \sum|F_o - F_c|/\sum F_o = 0.047$ and $R_2 = (\sum w(F_o^2 - F_c^2)^2/\sum w(F_o^2)^2)^{1/2} = 0.115$.

The standard deviation of an observation of unit weight was 1.03. The highest peak in the final difference Fourier had a height of 0.81 e/A^3. The minimum negative peak had a height of −0.55 e/A^3.

The factor for the determination of the absolute structure refined to 0.01.[41] Refinement was performed on a AlphaServer 2100 using SHELX-97.[36] Crystallographic drawings were done using programs ORTEP[37] and PLUTON.[38]

Acknowledgment. The authors gratefully acknowledge the National Science Foundation (CHE-9319173 and CHE-0315593) for support. G.M.F. wishes to thank the Department of Education for a predoctoral fellowship. L.M. wishes to thank Kalamazoo College for providing her with the opportunity to conduct her senior individualized project at Purdue University.

Supporting Information Available: Crystallographic data in CIF format. Variable temperature ^{1}H and ^{31}P NMR spectra for complex $\mathbf{6}^{2+}$ and solution ν(CN) stretching frequencies of **1**−**3**, **5**, **6**, and **8**. This material is available free of charge via the Internet at http://pubs.acs.org.

IC035021J